Dalton Transactions

RSC Publishing

PAPER

View Article Online
View Journal

Cite this: DOI: 10.1039/c3dt51429c

Activation of a (cyclooctadiene) rhodium(I) complex supported by a chiral ferrocenyl phosphine thioether ligand for hydrogenation catalysis: a combined *para*hydrogen NMR and DFT study†

Ekaterina M. Kozinets,[a,b,c] Marianna Fekete,[d] Oleg A. Filippov,[c] Natalia V. Belkova,*[c] Elena S. Shubina,[c] Rinaldo Poli,*[a,b,e] Simon B. Duckett*[d] and Eric Manoury*[a,b]

Received 31st May 2013,
Accepted 24th June 2013

DOI: 10.1039/c3dt51429c

www.rsc.org/dalton

The reaction of [RhCl(P,S^{t}Bu)(COD)] (**1**) or [Rh(P,S^{t}Bu)(COD)]BF_4 (**2**) where (P,S^{t}Bu) is CpFe[η^5-1,2-$C_5H_3(PPh_2)(CH_2S^tBu)$] with H_2 in MeOH gives rise to COD hydrogenation and formation of a solvent-stabilized product. The formation of hydride species cannot be observed in view of a very rapid H/D exchange between H_2 and the solvent. Introduction of pyridine or acetonitrile slows down this exchange process and allows observation of diastereometric dihydride complexes, $[Rh(P,S^tBu)(H)_2(L)_2]^+$, the stereochemistry of which was fully elucidated. The hydride site exchange rates have been derived from EXSY NMR experiments and used, with assistance from DFT calculation, to elucidate the isomerization and site exchange mechanisms.

Introduction

Square planar d^8 complexes of Rh^I and Ir^I are commonly employed as catalysts in a variety of hydrogenation processes. The most popular examples include the so-called "Wilkinson's catalyst", $[RhCl(PPh_3)_3]$,[1] and the cation $[Ir(COD)(L)_2]^+$ (L = PPh_3, $PMePh_2$, py), the latter of which displays high activities even with relatively hindered C–C double bonds.[2] Complexes of the type $[MCl(diene)]_2$ or $[M(diene)_2]^+$ [M = Rh or Ir], and particularly those of iridium, have also proven suitable as pre-catalysts for the ionic hydrogenation of polar substrates such as ketones and imines in the presence of appropriate ligands, mostly diphosphines.[3–10] A notable example of this is provided by Ir^I-catalyzed imine hydrogenation as used in the multi-ton scale industrial production of the herbicide metolachor.[11,12]

In one of our laboratories, chiral ferrocene-based phosphine thioether ligands (P,SR in Scheme 1)[13] have been developed and shown to be particularly efficient in terms of both activity and enantioselectivity for the hydrogenation of aromatic ketones when combined with $[IrCl(COD)]_2$.[14] The Ir^I coordination chemistry of these ligands has also been described.[15,16] Since the initial studies that were aimed at generating and characterizing the catalytically active species met with difficulty, our attention has more recently turned to the analogous (P,SR)-based rhodium complexes, inspired by reports of the isolation and characterization of related diphosphine-based complexes at the pre-catalyst activation stage.[17–20] We have thus synthesized and characterized complexes of the type [RhCl(P,SR)(diene)] and $[Rh(P,SR)(diene)]^+BF_4^-$ (diene = cyclooctadiene, COD; norbornadiene, NBD),[21] as shown in Scheme 1. These complexes have been demonstrated to act as both structural and functional mimics of the analogous Ir systems, although they show lower catalytic

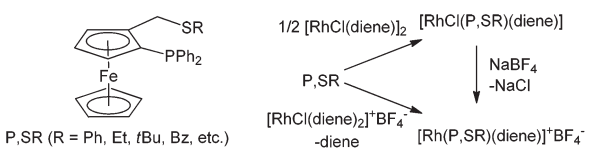

Scheme 1

[a]CNRS, LCC (Laboratoire de Chimie de Coordination), 205 route de Narbonne, BP 44099, F-31077 Toulouse Cedex 4, France CNRS.
E-mail: rinaldo.poli@lcc-toulouse.fr, eric.manoury@lcc-toulouse.fr;
Fax: +33-561553003; Tel: +33-561333173
[b]Université de Toulouse, UPS, INPT, F-31077 Toulouse Cedex 4, France
[c]A. N. Nesmeyanov Institute of Organoelement Compounds, Russian Academy of Sciences, Vavilov Street 28, 119991 Moscow, Russia. E-mail: nataliabelk@ineos.ac.ru; Fax: +7-499-1355085; Tel: +7-499-1356448
[d]Centre for Hyperpolarisation in Magnetic Resonance, Department of Chemistry, University of York, Heslington, York, YO10 5NY, UK.
E-mail: simon.duckett@york.ac.uk; Fax: +44 (0)1904-322516;
Tel: +44 (0)1904-322564
[e]Institut Universitaire de France, 103, bd Saint-Michel, 75005 Paris, France

†Electronic supplementary information (ESI) available: Sample preparation details for the parahydrogen NMR experiments, selected NMR spectra, description of the EXSY experiments of hydride exchange, figures of DFT optimized geometries and full table of Cartesian coordinates for the DFT optimized structures. See DOI: 10.1039/c3dt51429c

activity and selectivity.[22] We considered it of interest to investigate the phenomenon of precatalyst activation by the use of *para*hydrogen NMR.

The *para*hydrogen method has been used extensively to probe reaction mechanisms by enabling the detection of low concentration species such as intermediates in catalysis.[23,24] It was first successfully employed by Weitekamp,[25] and later Eisenberg and Bargon,[26] but is now being employed much more widely as a consequence of the potential that hyperpolarization methods offer to magnetic resonance imaging and hence health care.[27] When this approach is used in conjunction with DFT the synergy of the two methods becomes readily apparent as hitherto unseen species are not only predicted but firmly characterized in solution. Such studies have already been used to rationalize a series of reactions involving ruthenium clusters[28–30] where they can play a key role by helping with chemical shift and coupling assignments. Furthermore they have established a definitive opportunity to examine the role of electronic states in the oxidative addition of H_2 to a series of 16 electron ruthenium complexes[31,32] and aided in the understanding of hydrogenation catalysis by a range of palladium complexes,[33,34] and even to detect unexpected CH bond activation products in conjunction with the well-known complex $W(N_2)_2(dppe)_2$.[35]

In this contribution, we address the stoichiometric reactivity of two representative compounds containing the same (P,S^{t}Bu) ligand, [RhCl(P,S^{t}Bu)(COD)] (**1**) and [Rh(P,S^{t}Bu)(COD)]$^+BF_4^-$ (**2**), towards H_2 through the eyes of *para*hydrogen NMR, complemented by DFT calculations.

Experimental section

General

All the reactions described here and the complex purifications were carried out under argon using a high vacuum line or Schlenk line techniques. The Rh complexes [RhCl(P,S^{t}Bu)(COD)] (**1**) and [Rh(P,S^{t}Bu)(COD)]BF_4 (**2**) were synthesized from 2-diphenylphosphino-(*t*-butylthiomethyl)ferrocene (P,S^{t}Bu) and $[RhCl(COD)]_2$ or $[Rh(COD)_2]BF_4$ according to the published procedure.[21]

NMR experiments

NMR measurements were made using NMR tubes that were fitted with J. Young's valves and solutions were degassed on a high vacuum line prior to H_2 addition. The samples were prepared in a glovebox by addition of the specified deuterated solvents to the solid complex in the NMR tube. For the *p*-H_2 induced polarization (PHIP) experiments, hydrogen enriched in the para spin state was prepared by cooling H_2 to 36 K over the paramagnetic catalyst Fe_2O_3 which was doped on silica.[23,24,36] All the resulting NMR studies were then carried out with sample concentrations of approximately 4.6 mM and all spectra were recorded on a Bruker Avance III 400 NMR spectrometer. ^{1}H NMR chemical shifts are reported in ppm relative to the residual ^{1}H signal of the solvent which for CHD_2OD is δ 3.31 and for $CDHCl_2$ is δ 5.37. Further details can be found in the ESI.†

Computational details

Calculations were performed with the Gaussian09 package[37] using the B3LYP[38,39] and M06[40] functionals under the DFT approach. All carbon and hydrogen atoms were described with the 6-31G(d,p) basis set, whereas the 6-31++G(d,p) basis set was applied to the atoms of ligands involved in the bonding with Rh (P, S atoms, hydride ligands, the OH group of methanol and N atoms of pyridine and acetonitrile). Effective core potentials (ECP) and its associated SDD basis set[41–44] supplemented with f-polarization functions (SDD(f))[45] were applied to the Rh and Fe atoms. Geometry optimizations were performed without any ligand simplification for the cationic $[Rh(P,S^tBu)L_2]^+$ and $[Rh(P,S^tBu)(H)_2L_2]^+$ complexes (L = pyridine, CH_3OH, CH_3CN).

Frequency calculations were performed for all optimized complexes in the gas phase and reported without the use of scaling factors. The nature of all the stationary points on the potential energy surfaces was confirmed by a vibrational analysis.[46] Transition state (TS) structures showed only one negative eigenvalue in their diagonalized force constant matrices, and their associated eigenvectors were confirmed to correspond to the motion along the reaction coordinate under consideration using the Intrinsic Reaction Coordinate (IRC) method.[47]

Results and discussion

(a) NMR experiments

In CD_3OD without additives. The addition of *p*-H_2 to d_4-methanol solutions of either [RhCl(P,S^{t}Bu)(COD)] (**1**) or [Rh(P,S^{t}Bu)(COD)]BF_4 (**2**), over the temperature range 233–298 K, failed to result in the observation of any detectable hydride containing species. There was, however, evidence for a common slow reaction (*ca.* 18% conversion in 20 minutes at 243 K) which transformed the η^2–η^2-COD ligand into a $\kappa^3(\sigma{:}\pi)$ cyclooct-4-enyl ligand and generated the new proton loss complex, **3**, (Scheme 2) in very small amounts. The κ^3-ligand in this complex is characterized by features at δ 4.62, 1.54 and 2.15, see Fig. S1 and S2.† This suggests that while slow H_2 addition to the Rh centre occurs, rapid reaction transforms the resulting dihydride into **3**. This process is followed by reprotonation to form the corresponding alkene after hydride migration as shown in Scheme 2. The liberation of either HCl or HBF_4 is proposed to give **3**. Sola *et al.* have reported a related H_2 addition to the complex [Ir(COD)(NCCH$_3$)(PMe$_3$)]BF_4, where the initial dihydride product [Ir(H)$_2$(COD)(MeCN)(PMe$_3$)]BF_4 (in CH_2Cl_2) reacts with MeCN to form the monohydride product [IrH(1-κ-4,5-η-C$_8$H$_{13}$)(NCCH$_3$)$_2$(PMe$_3$)]BF_4. In this case, these species could be isolated and fully characterized.[48] We note that **3** is related to this Ir system by the formal loss of a proton. Given that Rh^{III} hydride complexes are known to be less stable than their Ir^{III} analogues, this transformation is not unexpected.

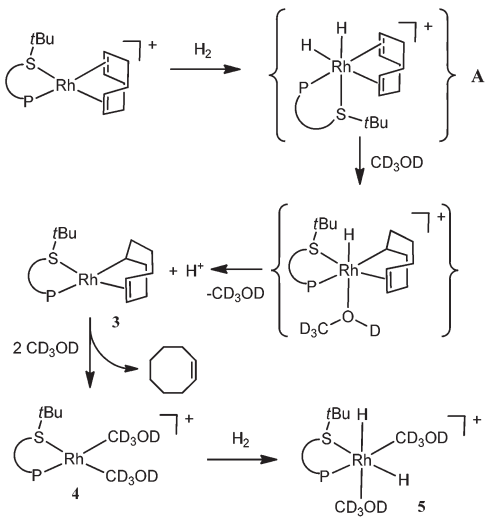

Scheme 2

At 253 K the generation of cyclooctene was revealed by its characteristic ^{1}H NMR resonance at δ 1.21, which rapidly increases in intensity over the time scale of 17 minutes (Fig. S2†). This demonstrates that the initial H_2 addition to **1** or **2** proceeds at 253 K. When the temperature was raised to 263 K the formation of cyclooctane was also observed through its characteristic singlet at δ 1.50. Hydride resonances were not observed at any time during this reaction. However, the residual OH signal of methanol and the H_2 signal show a dramatic temperature dependence, coalescing at 263 K, thereby suggesting the rapid interchange of these sites, presumably through the formation of transient, non-observable hydride species.

At 273 K the deuteration of the H_2, forming HD, becomes evident (Fig. S3†). In addition, the phenyl proton signals for the phosphine become more complicated in appearance at this point. This reaction monitoring demonstrated the instability of **3** and suggested that the ultimate formation of a bis(solvent) adduct, $[Rh(P,S^tBu)(MeOH)_2]^+$, **4**, takes place even though direct evidence for the production of this complex could not be obtained. Further H_2 oxidative addition to yield a putative dihydride species **5** appears excluded by the absence of hydride signals in this experiment (however, see additional discussion below). Monitoring the reaction carried out with regular H_2 at 5 bar pressure and room temperature by ^{31}P NMR did not result in the appearance of any new resonance, in fact only the signal for unreacted starting material could be seen even after 7 h. After 3 days the starting material was completely consumed and the new NMR spectrum shows very few small resonances, the major one being a doublet at δ 43.9 (J_{PRh} = 134.1 Hz). These data suggest that **4** is not stable.

Our attempts to isolate the final product of this reaction in a crystalline form have so far not succeeded. Heller *et al.* have recently reported the successful generation and isolation of the complex $[Rh(BINAP)(MeOH)_2]^+$ by hydrogenation of $[Rh(BINAP)(COD)]^+$ or $[Rh(BINAP)(NBD)]^+$ in methanol, although no reaction intermediates were observed in those cases.[18]

When this reaction was carried out in CD_2Cl_2 using **2**, reaction with *p*-H_2 was evident at temperatures down to 233 K. Under these conditions weak signals for a new hydride containing species were detected at δ −9.7 and −23.0. The high field signal yielded a ^{31}P coupling of 188 Hz which is indicative of a *trans* ^{31}P splitting. These two resonances were broad and neither the J_{HH} nor the J_{RhH} couplings could be quantified. In the corresponding ^{31}P decoupled spectra the δ −23.0 signal yields a J_{HH} splitting of −9 Hz and a J_{RhH} splitting of 20 Hz. The signals for this species were too weak to enable its characterisation but the hydride *trans* to phosphine deduction is confirmed by the large coupling and a species such as **A** in Scheme 2 is possible. The addition of 1 μl of MeOH to this solution suppressed the observation of these signals.

Two key observations outlined above (the coalescence of the MeOH and H_2 signals, and H/D exchange between these two molecules) led us to speculate on the mechanism associated with these phenomena, which are obviously related to the same process, occurring rapidly on the NMR timescale. Two possible pathways are indicated in Scheme 3. In pathway a, H_2 oxidative addition yields a Rh^{III} dihydride species **5** that would be sufficiently acidic to release a proton to the solvent and yield a Rh^I monohydride intermediate **6**. Reversal of all steps with the implication of deuteron incorporation is a consequence of this exchange pathway. In the alternative pathway b, H_2 replaces a methanol ligand to yield an H_2 complex (non-classical dihydride) **7**, which is then deprotonated by the solvent to yield the same monohydride complex **6** as detailed above. Both of these pathways can be imagined to occur *via* initial reaction which places the hydride *trans* to S (as shown in Scheme 3) or in the alternative position *trans* to P which is not illustrated. Incidentally, the lack of observation of a hydride resonance under these conditions does not exclude the fact that the most stable species (at least at low temperatures) is indeed a mono- or dihydride complex, since such a species would exist primarily in the form of a deuteride and would therefore be unobservable in the hydride region of the ^{1}H NMR spectrum.

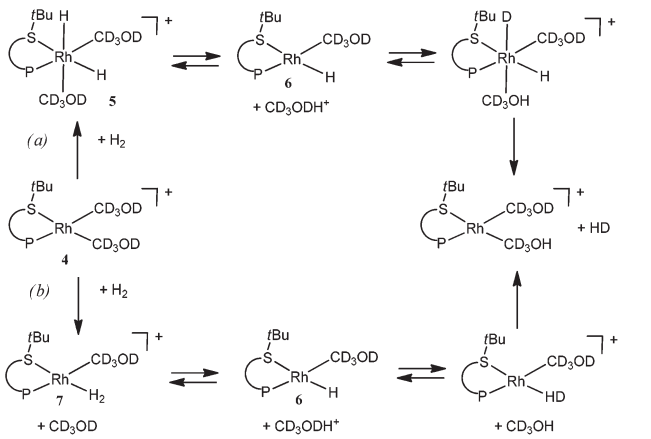

Scheme 3

In CD_3OD in the presence of pyridine. When the analogous reactions of either **1** or **2** with H_2 were carried out in the presence of pyridine at low temperature (233–283 K), on the other hand, two common and dominant hydride containing products formed. For example, when a d_4-methanol solution of **1** was prepared which contained a 75-fold excess of pyridine (75 equiv.) and the resulting reaction with p-H_2 was monitored by ^{1}H NMR spectroscopy at 233 K, four PHIP enhanced hydride signals were observed at δ −13.1, δ −14.3, δ −17.2 and δ −17.6. These hydride ligand signals all contained anti-phase features due to their formation from p-H_2 that are associated with their common J_{HH} coupling in addition to in-phase splittings due to further couplings to a single rhodium and a single phosphorus centre. A more complete NMR monitoring of this reaction was undertaken after warming the sample to 263 K, during which process the NMR spectral features did not change. The hydride region of the resulting ^{1}H NMR spectrum is shown in Fig. 1a. The J_{PH} coupling values are all consistent with *cis* hydride phosphorus ligand arrangements. In addition, in the corresponding ^{1}H–^{31}P HMQC NMR spectrum (Fig. 1b), the δ −13.1 (J_{HH} = −13 Hz, J_{RhH} = 24 Hz) and δ −17.6 (J_{HH} = −13 Hz, J_{RhH} = 19 Hz) signals proved to couple to a single ^{31}P centre that was located at δ 47.9 and appeared with a J_{RhP} of 140.0 Hz. These resonances therefore arise from groups within the same complex (**8**). In a similar manner the δ −14.3 (J_{HH} = −10 Hz, J_{RhH} = 24 Hz) and δ −17.2 (J_{HH} = −10 Hz, J_{RhH} = 20 Hz) signals arise from a second species (**9**) where now the connected ^{31}P resonance appears at δ 45.0 with a J_{RhP} of 141.6 Hz. On the basis of the relative hydride resonance peak areas it can be suggested that **8** and **9** are formed in a step which shows a kinetic selectivity of approximately 1 : 4 at 233 K, if it is assumed that these resonances result from PHIP derived magnetic states that are created with identical efficiency. When the temperature is raised to 273 K, the ratio increases to 1 : 13.

Upon increasing the solution temperature to 283 K, no change in the relative size of the PHIP-enhanced signals was observed. However, upon warming to 298 K and beyond, the hydride signals for **8** and **9** could no longer be observed. When this experiment was repeated at 263 K with normal dihydrogen, the ratio of the hydride signals of **8** and **9** was 1 : 7. When, on the other hand, the reaction was conducted at room temperature (*ca.* 15 min between bubbling and recording the NMR spectrum), only the presence of compound **9** could be

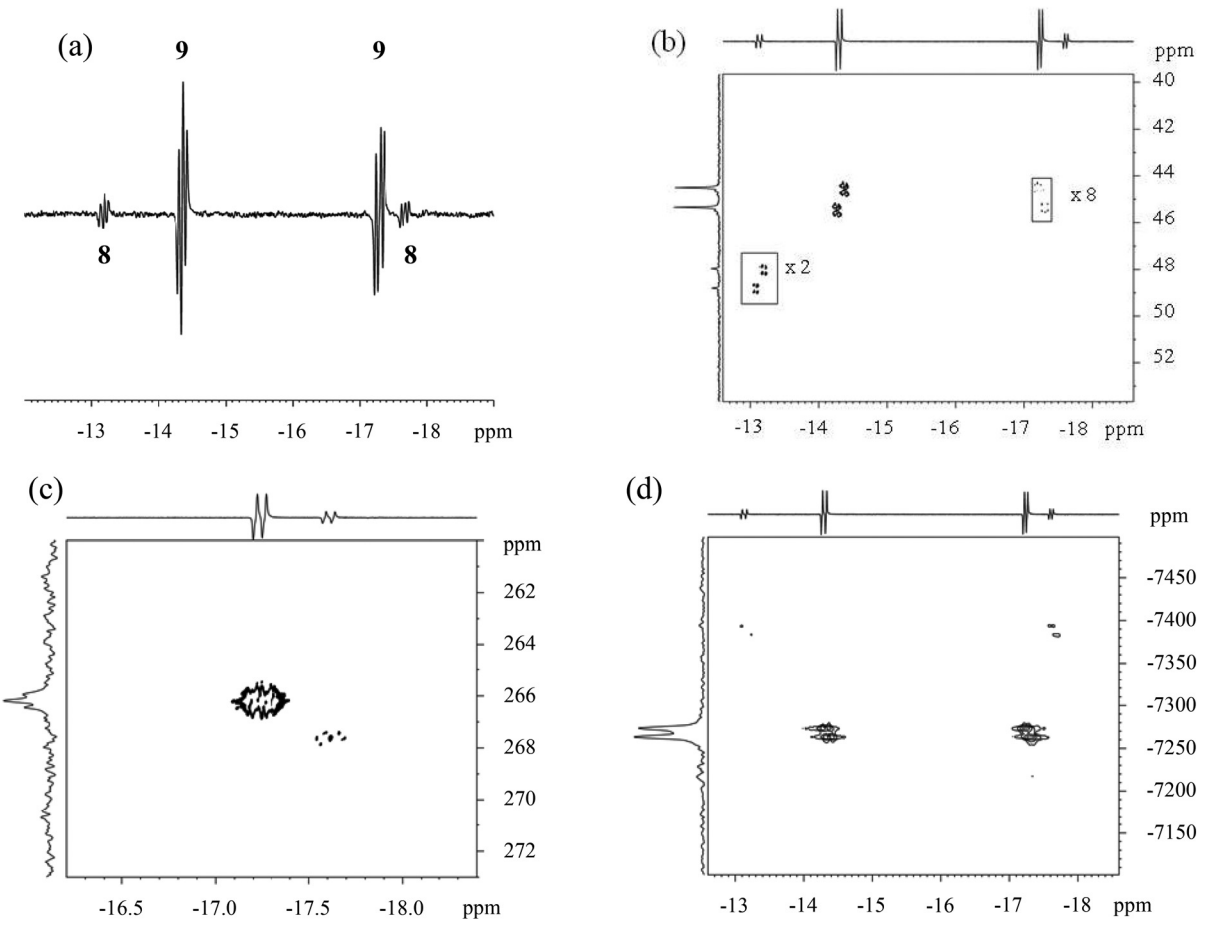

Fig. 1 NMR spectra showing characteristic resonances of **8** and **9** (as indicated) observed during reaction of **2** in d_4-methanol with p-H_2 and 75 equiv. of pyridine at 263 K: (a) p-H_2 enhanced ^{1}H NMR spectrum showing the hydride region; (b) ^{1}H–^{31}P HMQC NMR spectrum collected using ^{15}N labeled pyridine; (c) ^{15}N labeled, ^{1}H–^{15}N HMQC NMR spectrum; (d) ^{1}H–^{103}Rh HMQC NMR spectrum (in (b) the inset boxes reflect vertical expansions of ×2 and ×8 relative to the baseline).

Table 1 NMR data for complexes **8** and **9** in MeOD at 283 K

Compound	δ ^{1}H	δ ^{31}P	δ ^{15}N	δ ^{103}Rh
8	−13.1, dd, J_{HH} = −13 Hz; J_{RhH} = 24 Hz, J_{RhP} = 140.0 Hz −17.6, dd, J_{HH} = −13 Hz; J_{RhH} = 19 Hz, J_{RhP} = 140.0 Hz	47.9, d	267.6, t, J_{PN} = 50 Hz; J_{NH} = 20 Hz	−7390, d J_{RhP} = 131 Hz
9	−14.3, dd, J_{HH} = −10 Hz; J_{RhH} = 24 Hz, J_{RhP} = 141.6 Hz −17.2, dd, J_{HH} = −10 Hz; J_{RhH} = 20 Hz, J_{RhP} = 141.6 Hz	45.0, d	266.2, t, J_{PN} = 50 Hz; J_{NH} = 20 Hz	−7268, d J_{RhP} = 131 Hz

detected, reflecting the greater thermodynamic preference for this isomer.

In order to probe the ligand arrangement in compounds **8** and **9** further, a ^{15}N labelled pyridine sample was examined. Now, the two phosphorus signals associated with these two complexes exhibit additional and identical extra splittings of 50 Hz due to the presence of a resolved *trans* ^{31}P–^{15}N coupling. In the corresponding ^{1}H–^{15}N HMQC NMR spectrum (Fig. 1c), the hydride signals at δ −17.2 and −17.6 showed strong correlation peaks to ^{15}N resonances at δ 266.2 and δ 267.6 respectively. In addition, a hydride-^{15}N splitting of 20 Hz was exhibited by the two low field hydride resonances of **8** and **9**. Rhodium signals have also been detected at δ −7268 for **8** and δ −7389 for **9** through the recording of a ^{1}H-^{103}Rh HMQC spectrum as shown in Fig. 1d.

This information therefore confirms that there are two pyridine ligands attached to the metal centre in **8** and **9**, which are located *trans* to one hydride and to the phosphine donor. Given the bidentate nature of the P,S ligand it can be further concluded that the second hydride ligand in both **8** and **9** is *trans* to sulfur. All the NMR data associated with **8** and **9** resulting from this study are summarized in Table 1. The similarity of these NMR data suggests that these two products are simply diastereoisomers of one another, differentiated by the ferrocene ligand orientation as shown in Scheme 4. This product geometry indicates that the initial H_2 oxidative addition takes place over the S–Rh–C axis.

When an nOe experiment was recorded to probe the hydride site interchange process undergone by these complexes at 273 K with the 75-fold excess of pyridine, several exchange processes were observed (as revealed in Fig. 2). These include a mutual hydride site interchange within **9** which proceeds with an exchange rate constant of 0.785(6) s^{-1} and the interconversion of **9** into **8** on a slower timescale that places the moving hydride into either site of **8** with rates of 0.167(2) s^{-1} where H_c becomes H_a and H_d becomes H_b and 0.160(3) s^{-1} where H_c becomes H_b and H_d becomes H_a. Hence there is a limited selectivity in this process. Isomer **8** converts into **9** on a faster timescale where the observed rate constant is 1.10(1) s^{-1} for the $H_{a\rightarrow d}$ and $H_{b\rightarrow c}$ transformations and 1.19(1) s^{-1} for the $H_{a\rightarrow c}$ and $H_{b\rightarrow d}$ transformations. The experimental rate constant for hydride site interchange in **8** is zero. The overall scheme of hydride site exchange rates is summarized in Scheme 5. Table S1 (ESI†) shows the list of constraints that were used for the calculation of the exchange rate constants. There was no evidence for hydride exchange into free H_2 or MeOH from **8** or **9** in these experiments which are limited by the timescale of NMR relaxation, and contrary to the

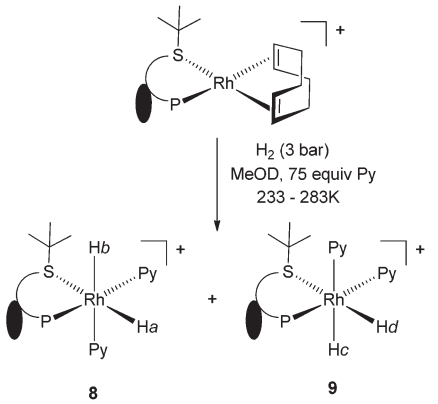

Scheme 4

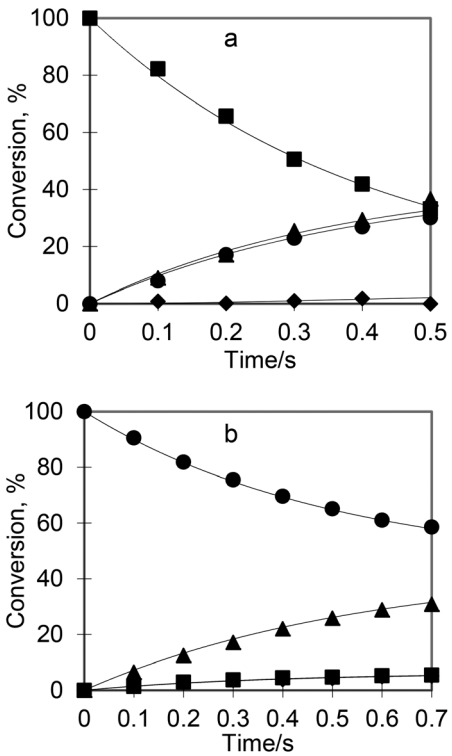

Fig. 2 Hydride ligand exchange data for the interconversion of **8** and **9** in the presence of 75-fold excess of py, as probed through the selective excitation of (a) H_a of **8** and (b) H_c of **9**, over the defined observation period; the observation points are listed as H_a (■), H_b (◆), H_c (●) and H_d (▲) as defined in Scheme 4. The solid lines correspond to simulated changes that yield the rate constants in the text.

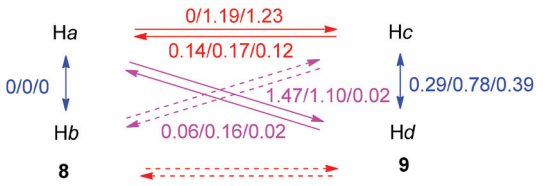

Scheme 5 The three numbers on each arrow are the exchange rates in s^{-1} relative to the solution with an 8-fold, 75-fold and 173-fold excess of py.

experiment run in pure CD_3OD there was no coalescence between the solvent and H_2 resonances. We note, however, that the hydride sites of **8** and **9** are partially deuterated in these experiments. This readily shows up in a ^{31}P-decoupled HMQC measurement as isotopically perturbed signals at δ −13.1, −14.3, −17.2 and −17.6 in the corresponding ^1H NMR spectrum for the Rh(H)(D) partners and at δ −14.3 and δ −17.2 for the corresponding ^{31}P signals. Hence, the electronic effect of pyridine coordination stabilizes the dihydride species against deprotonation (*cf.* Scheme 3).

While the deuterium label incorporation into the hydride sites is relatively slow, it precludes the measurement of precise rate data as would be required for the assembly of an Eyring plot. Nonetheless, the interconversion between these species has been defined as occurring without H_2 loss. This is reflected in the fact that strong PHIP is only seen when **1** or **2** are being converted into **8** and **9**. When we monitor these processes with differing amounts of pyridine, changing the Rh/pyridine ratio from 1 : 8 to 1 : 75 and 1 : 173, we see no change in the relative hydride signal intensities of **8** and **9**. There is, however, a significant effect on the hydride site interchange rate constants.

The rate constant for the mutual hydride site exchange in **9** falls to 0.29 s^{-1} with an 8-fold excess of pyridine while it is 0.39 s^{-1} with a 173-fold excess. The kinetic effect of pyridine is therefore complex, first promoting the process and then inhibiting it. A similar trend is observed for the $H_{d\rightarrow a}$ (and $H_{c\rightarrow b}$) rate from 0.06 s^{-1} through 0.16 s^{-1} to 0.02 s^{-1} and for the $H_{c\rightarrow a}$ (and $H_{d\rightarrow b}$) rate from 0.14 s^{-1} through 0.17 s^{-1} to 0.12 s^{-1}, though the effect here is less dramatic. In contrast, the $H_{a\rightarrow c}$ ($H_{b\rightarrow d}$) process shows a rate increasing with [py] from 0 s^{-1} through 1.19 s^{-1} to 1.23 s^{-1} while the rate of the $H_{a\rightarrow d}$ ($H_{b\rightarrow d}$) process shows the opposite trend from 1.47 through 1.10 to 0.02 s^{-1}. We can conclude therefore that pyridine plays a role in these processes. All observed hydride site exchange rate constants are collected in Table S3.†

The hydride signal at δ −17.2 shows nOe connections to peaks at δ 8.71, 8.23, 4.67, 3.84 and 1.21, which are due to the *ortho* proton of a pyridine ligand, the *ortho* proton of the phosphine, the ferrocenyl group and the ^{t}Bu group in **9**. The second hydride signal in **9** which resonates at δ −14.3 shows through space interactions with protons that give rise to resonances at δ 8.71, 8.31, 8.23 and 6.68. The extra signal at δ 8.31 is therefore the *ortho* proton of a second pyridine ligand. In the corresponding ^1H–^{31}P HMQC, the ^{31}P centre which resonates at δ 45.0 connects to two aromatic signals at δ 8.23 and 6.78. In contrast, the ^{31}P signal of the minor isomer **8** proved to connect with ^1H signals at 8.03 and 7.5 in an HMQC measurement. Furthermore, nOe data confirmed that the signal at δ −13.1 in **8** connect with ^1H signals at δ 8.42 and 8.03. The δ 8.42 resonance therefore corresponds to an ortho-pyridine signal. This information has therefore confirmed the assignment shown in Scheme 4. The structure corresponding to **9** has therefore the hydride ligand *trans* to pyridine located on the same side as the ferrocenyl group. When a long range ^1H–^{31}P experiment was recorded, further proton signals were located at δ 7.6, 4.8 and 4.2 in **9**.

The hydrogenation of the cyclooctadiene ligand is readily evident in these *p*-H_2 enhanced ^1H NMR spectra from 253 K. Two sets of polarised signals appear at δ 1.53 and 1.50 due to the CH_2 protons of the hydrogenated components of COE. A further resonance is evidenced at δ 1.41 for the backbone signals as described above. In these ^1H NMR spectra the corresponding cyclooctane signal appears at δ 1.2 and forms very slowly at 273 K.

When the reaction of the chloride derived precursor **1** with normal dihydrogen is monitored in an analogous experiment with only a 15-fold excess of pyridine (instead of 75 in the experiment described above), **5** appears as the first formed hydride containing product at 273 K. The problem with this measurement is, however, that it relies on detecting a weak signal from magnetisation that is at thermal equilibrium. When this reaction is repeated with *p*-H_2, weak PHIP-enhanced hydride signals are now seen for a further two species, **10** and **11**, besides those of **8** and **9** in the resulting NMR spectra at 273 K (Fig. 3). The hydride signals of **10** appear at δ −12.3 and −18.7 with Rh–H couplings of 25.1 Hz and 26.8 Hz, respectively, and a common J_{HH} coupling of −5.9 Hz. The hydride ligand signals from species **11** are, however, much weaker than those of **10** and appear at δ −15.0 (J_{RhH} = 20, J_{HH} = −9 Hz) and δ −17.8 (J_{RhH} = 15, J_{HH} = −9 Hz). The relative ratio of the hydride signals for **10**, **8**, **9**, and **11** proved to be 0.9 : 7.0 : 39.6 : 1 at 273 K. In a series of 2D measurements the δ −12.3 hydride signal proved to connect with a δ 34.3 ^{31}P

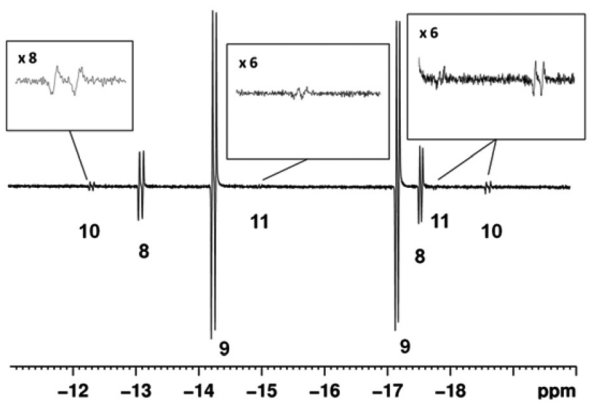

Fig. 3 NMR spectra showing characteristic hydride resonances of **8**, **9**, **10** and **11** (as indicated) observed during reaction of **1** in d_4-methanol with *p*-H_2 and 45-fold excess of pyridine at 273 K.

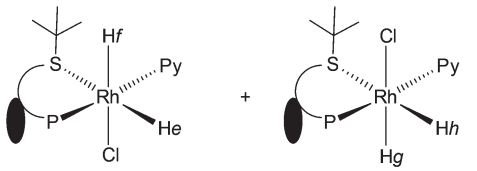

10 11

Scheme 6

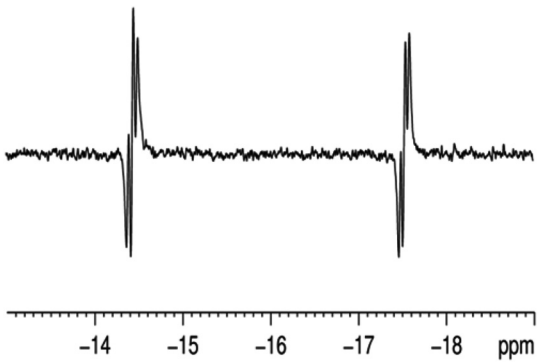

Fig. 4 p-H_2 enhanced ^{1}H NMR spectrum showing the hydride region of **12** observed during reaction of **1** in d_4-methanol with p-H_2 and acetonitrile at 273 K.

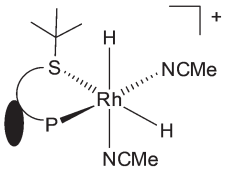

12

Scheme 7

resonance where J_{RhP} = 140 Hz, while the δ −15.0 hydride signal connects with a ^{31}P resonance at δ 51.4 that exhibits a J_{RhH} coupling of 148 Hz. The relative intensity of the signals for **10** and **11** proved to fall as the excess of pyridine is increased. When labelled pyridine is employed, both of the sets of hydride signals show limited broadening but no *trans*-^{15}N coupling is evident. We therefore assign **10** and **11** to chloride containing [Rh(H)$_2$(P,SR)(pyridine)Cl] as shown in Scheme 6. This deduction is further supported by the fact that while the relative intensities of the signals for **8** and **9** seem to remain constant regardless of the [py], those for **10** and **11** drop as the [py] increases.

When a series of EXSY measurements were undertaken to examine the dynamic behaviour of this complex reaction system, interconversion between **10**, **8** and **9** was evident with the signals for **11** proving to be too weak to monitor.

When the pyridine excess was 75 fold, the experimental rate constant for the $H_{e\rightarrow c}$ and $H_{e\rightarrow d}$ processes (**10** → **9**) were indistinguishable at 31 s^{-1}. In contrast the corresponding rate constant for $H_{e\rightarrow a}$ and $H_{e\rightarrow b}$ (**10** → **8**) was zero, as was mutual H_e–H_f interchange (**10**). These values decrease from 31 s^{-1} to 20 s^{-1} to 3 s^{-1} as the pyridine excess falls from 75 fold through 42 fold to 15 fold. Hence this process is [py] dependent. Concerning the **9** → **10** process, the $H_{c\rightarrow e}$ rate constant is 0.41 s^{-1}, and the $H_{c\rightarrow f}$ rate has a similar value. The corresponding rates for the **9** → **8** process are slightly smaller than those found when **2** is employed ($H_{c\rightarrow a}$ and $H_{c\rightarrow b}$ are again similar at 0.1 s^{-1} *vs.* 0.16 s^{-1} for **2**). The new rate constants for **8** → **9** with hydride position retention are zero when **1** is the precursor and 1.1 s^{-1} when **2** is employed. **8** does, however, form **10** with rate constants 1.3 s^{-1} for $H_{a\rightarrow f}$ and zero for $H_{a\rightarrow e}$. The observed hydride site exchange rate constants at 273 K measured on sample **1** for different pyridine concentrations are reported in Table S2.†

In CD_3OD in the presence of acetonitrile. In a further study, a d_4-methanol sample of **1** containing 20 μL of acetonitrile was prepared. No reaction of **1** with H_2 was evident until 273 K. At this point, the corresponding ^{1}H NMR spectrum contained two PHIP polarized hydride peaks at δ −14.5 and −17.6. These hydride signals again appear as simple anti-phase doublets with additional phosphorus and rhodium couplings (Fig. 4). The signal at δ −14.5 exhibits a J_{HH} coupling of 11 Hz, a J_{HP} coupling of 20 Hz and a J_{RhH} coupling of 21 Hz while the corresponding splittings of the δ −17.6 signal are 12, 17 Hz and 20 Hz respectively. In the corresponding ^{1}H–^{31}P HMQC NMR spectrum, the δ −14.5 signal and the δ −17.2 signal proved to couple to a single ^{31}P centre located at δ 47.6 which exhibited a J_{RhP} splitting of 148 Hz. These results suggest that hydrogenation of **1** in the presence of acetonitrile selectively forms the MeCN analogue (**12**) of **8** (Scheme 7). There are a number of similarities between these data and those of **8**. For example, all the couplings suggest a *cis* PH ligand arrangement and the chemical shifts are reflective of hydride ligands *trans* to sulfur and nitrogen. The coordination of MeCN has therefore the same effect as that of pyridine in reducing the hydride acidity and reducing the speed of the H/D exchange between H_2 and the solvent.

Hydrogenation studies. We have also explored the activity of these systems as hydrogenation catalysts. When a d_4-methanol sample of **1** containing 20 μl (75 equiv.) of pyridine and diphenylacetylene was examined at 258 K, limited hydrogenation was evident and strongly enhanced signals for **8**, **9**, **10** and **11** were visible which exceed those in the analogous experiment without the alkyne. Under these conditions at 258 K the ratio of the p-H_2 enhanced hydride signals of **8** and **9** was now 1 : 3.8. In contrast, when a similar sample was examined without pyridine, more rapid, but still slow, hydrogenation of diphenylacetylene occurs; signals for both *cis* and *trans* stilbene are evident. These signals appear in an OPSY measurement which was used to detect only protons that were previously located in a single molecule of p-H_2. No hydride signals were observed during these measurements.

When hydrogenation of the more reactive substrate phenylacetylene by **1** was examined in d_4-methanol using p-H_2, PHIP polarized signals could be readily seen for the styrene product at 263 K when no pyridine was present. No hydride signals still

are visible however in this experiment. In contrast, when a 10-fold excess of phenylacetylene and acetonitrile was added there was evidence for both the formation of **12** and the hydrogenation of phenylacetylene.

(b) DFT calculations

On the basis of the presented experimental evidence, H_2 is able to hydrogenate the COD ligand in compounds **1** and **2** in MeOH, presumably yielding a $[Rh(P,S^tBu)(MeOH)_2]^+$ product (**4**). However, any further oxidative addition of H_2 to yield a putative dihydride product $[Rh(H)_2(P,S^tBu)(MeOH)_2]^+$ (**5**) would not be evidenced by ^1H NMR if there was rapid H/D exchange as suggested. On the other hand, further H_2 oxidative addition takes place in the presence of py or MeCN to produce observable dihydridorhodium(III) species. A first question addressed by the computation tool was to explore the relative stability of the $[Rh(P,S^tBu)L_2]^+$ (L = MeOH, py, MeCN) complexes and their ability to oxidatively add H_2, as well as defining the relative stability of all possible product isomers, see Scheme 8. The associated calculations were carried out using either the B3LYP functional or the M06 functional.

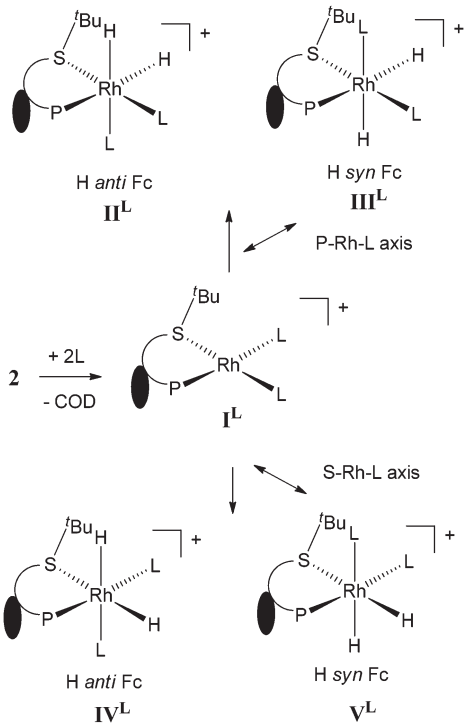

Scheme 8

The hypothetical replacement of the COD ligand in $[Rh(P,S^tBu)(COD)]^+$ (**2**) with two L donors to yield $\mathbf{I^L}$ (without COD hydrogenation) was found at the B3LYP level as endoergic when L = MeOH (ΔE = 15.4 kcal mol^{-1}, ΔG = 24.7 kcal mol^{-1}) and more favourable for the other two ligands ($\Delta E/\Delta G$ are −6.4/+4.4 kcal mol^{-1} for L = py and −1.5/+6.0 for L = MeCN). However, in consideration of the energy gain of the COD hydrogenation process (ΔE = −34.4 or ΔG = −18.5 kcal mol^{-1} for the hydrogenation to cyclooctene; ΔE = −64.3 or ΔG = −33.1 kcal mol^{-1} for the hydrogenation to cyclooctane), all the underlying reactions become favourable.

The oxidative addition of H_2 was also found to be energetically favourable for all three ligand systems, as shown by the data collected in Table 2. It should be noted that while the gas phase free energies are positive, the computed values do not take into account stabilisation from solvation and the partial quenching of translational and rotational modes in the condensed phase. Furthermore, the hydride complexes were observed at low temperatures, where the detrimental effect of the positive $T\Delta S$ contribution is smaller (for instance, the calculated ΔG for the oxidative addition to $\mathbf{I^{py}}$ to yield $\mathbf{V^{py}}$ at the M06 level decreased from +6.0 to +4.9 kcal mol^{-1} when applying the thermochemical corrections at 253 K instead of 298 K) and indeed the hydride resonances were lost upon warming the NMR tubes to higher temperatures (*vide supra*). For the pyridine system, the calculations have also been carried out at the M06 level, showing a slightly less favourable process. We note that the oxidative addition process for L = MeOH is predicted by these calculations to be more favourable than for the other two ligands. Therefore, failure to observe the corresponding hydride resonances by ^1H NMR during the experiments appears indeed to be attributable to the accumulation of deuteride species by rapid H/D exchange. The dihydride complex is, however, at least sufficiently accessible to allow the H/D process to take place as suggested in Scheme 3.

The computational results also suggest that the two isomers resulting from the H–H addition across the S–Rh–L axis are energetically preferred independent of L, in agreement with the assignment of the NMR spectra. The stereochemistry of structure **IV** corresponds to that of **8** and **12** and the stereochemistry of **V** corresponds to that of **9**. Structure $\mathbf{V^{py}}$ is slightly less stable than $\mathbf{IV^{py}}$ at the B3LYP level, but more stable at the M06 level in agreement with the NMR evidence. For L = MeCN and MeOH, the calculations also indicate greater stability for isomer $\mathbf{V^L}$ even at the B3LYP level, whereas the NMR assignment indicates that the observed compound **12** has the same configuration as **IV**.

Table 2 Relative gas phase energies *E* (free energies *G* in parentheses) in kcal mol^{-1} for the products of H_2 oxidative addition to $\mathbf{I^L}$

L	Functional	$\mathbf{II^L}$	$\mathbf{III^L}$	$\mathbf{IV^L}$	$\mathbf{V^L}$
MeOH	B3LYP	−8.5(+2.6)	−10.5(+1.3)	−14.1(−2.5)	−17.6(−6.5)
Py	B3LYP	−4.5(+7.4)	−4.9(+7.9)	−10.1(+1.5)	−10.0(+2.1)
Py	M06	+4.5(+15.2)	+2.2(+14.7)	−2.5(+7.8)	−3.5(+6.0)
MeCN	B3LYP	−4.2(+5.6)	−4.9(+6.0)	−8.5(+1.7)	−10.9(−0.1)

A second question addressed by the DFT study is the mechanism for the H-site exchange in the two observed isomers for the pyridine systems (**8** and **9**, or $\mathbf{IV^{py}}$ and $\mathbf{V^{py}}$). The simplest way to imagine the isomerisation process, given the known strong *trans* labilizing effect of the hydride ligands, involves dissociation of a neutral donor placed *trans* to a hydride ligand (either the sulphur donor of the bidentate P,S ligand or a pyridine molecule) and rearrangement of the coordination sphere, as shown in Scheme 9 for the specific case of thioether dissociation. The putative 5-coordinate intermediate **A** would then rearrange to its diastereoisomer **B** (the same chirality at ferrocene and inverted chirality at rhodium) by either concerted hydride migration and rotation of the P,S ligand or *via* tautomerization to the dihydrogen complex **C** followed by P,S rotation to yield the rotamer **D**. Hydride site exchange can be envisaged by rotation of the dihydrogen ligand in the intermediates **C** and **D**. The observation of such a ligand exchange process by NMR is not inconsistent provided the lifetime of the rapidly relaxing dihydrogen form is short.[23,24]

All calculations of this pathway were carried out with the M06 functional, since this is expected to better handle the long range dispersion interactions involved in the ligand dissociation processes. They show that pyridine dissociation is less favourable than the P,S ligand thioether arm dissociation. The most favourable dihydride complex resulting from py dissociation, $[(P,S^tBu)Rh(H)_2(py)]^+$, is located at 29.7 kcal mol^{-1} from $\mathbf{V^{py}}$, while the isomeric non-classical complex $[(P,S^tBu)Rh(H_2)(py)]^+$ is more stable at only 18.3 kcal mol^{-1} from $\mathbf{V^{py}}$. However, the most stable dihydride complex resulting from dissociation of the thioether arm (**B** in Scheme 9) is only 12.4 kcal mol^{-1} from $\mathbf{V^{py}}$, with **A** being only slightly higher at +14.7 kcal mol^{-1} and the nonclassical isomers **C** and **D** are even more stabilized at +11.8 and +8.3 kcal mol^{-1}, respectively. Therefore, the isomerization pathway shown in Scheme 9 was fully explored. The results are summarized in Fig. 5. Rearrangement of the classical to the nonclassical dihydrides occurs *via* localized transition states $\mathbf{TS_{AC}}$ and $\mathbf{TS_{BD}}$ at +18.4 and +16.2 kcal mol^{-1}. A more direct pathway from $\mathbf{IV^{py}}$ to **C** and from $\mathbf{V^{py}}$ to **D** could not be found. The P,S ligand rotation pathway involved in the interconversion of **C** and **D** was not straightforward to investigate for the location of a stationary point, but a manual scan of the dihedral N–Rh–P–C angle (see Fig. S4†) led to the identification of a new local minimum corresponding to a new rotational intermediate **E** and two maxima, the highest point being 4.3 kcal mol^{-1} higher than **D** (+12.6 kcal mol^{-1} from $\mathbf{V^{py}}$). The search for a more direct pathway from **A** to **B** was unsuccessful. The barrier for site exchange was calculated for **D** and turned out rather low (2.5 kcal mol^{-1} or +10.8 kcal mol^{-1} from $\mathbf{V^{py}}$), lower than the barriers required to go back to the stable classical dihydride isomers.

The results in Fig. 5 are in agreement with certain experimental observations. Isomerization from $\mathbf{V^{py}}$ (**9**) to $\mathbf{IV^{py}}$ (**8**) requires transiting over the $\mathbf{TS_{AC}}$ barrier, whereas the site exchange in **9** may occur by simple access of the nonclassical intermediate and facile H_2 rotation, followed by the reverse pathway to $\mathbf{V^{py}}$ through the lower $\mathbf{TS_{BD}}$ barrier. This agrees with the faster site exchange relative to the **9** → **8** process. During the reverse isomerization of $\mathbf{IV^{py}}$ (**8**) to $\mathbf{V^{py}}$ (**9**), on the other hand, once the highest $\mathbf{TS_{AC}}$ barrier is passed and the intermediate **C** is generated, the isomerization process through P,S ligand rotation and the lower energy $\mathbf{TS_{BD}}$ occurs faster than the reverse generation of $\mathbf{IV^{py}}$, consistent with the fact that site exchange for **8** is not observed.

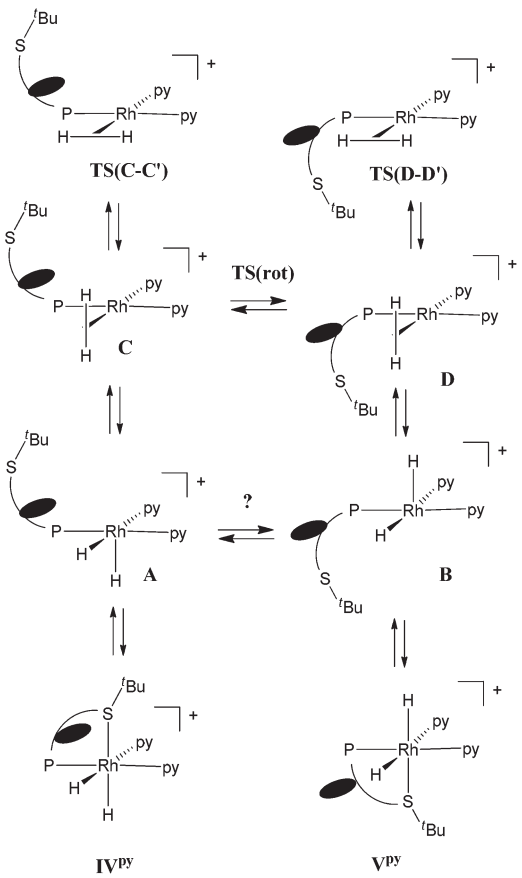

Scheme 9

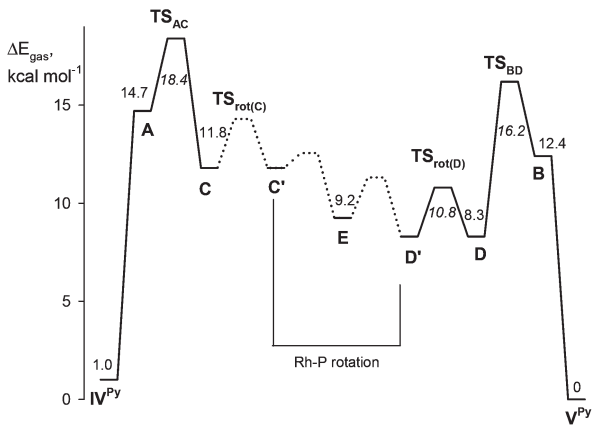

Fig. 5 Energy profile (gas phase energies in kcal mol^{-1}) of the isomerization pathway of Scheme 9.

A most interesting experimental result is that the transformation of the minor isomer (**8**) into the major one (**9**) occurs preferentially as $H_{a\rightarrow c}$ and $H_{b\rightarrow d}$ at low [py] but preferentially as $H_{a\rightarrow d}$ and $H_{b\rightarrow c}$ at high [py] (see Scheme 5). The former situation, according to Scheme 9, would be compatible with a concerted pathway directly converting **A** to **B** without transiting through the nonclassical intermediate (arrows with a question mark in Scheme 9) through a transition state at a lower energy than $\mathbf{TS_{AC}}$ and $\mathbf{TS_{BD}}$. As stated above, such a pathway could not be located but we cannot exclude that it exists. At greater pyridine concentrations, this pathway may be blocked by reversible coordination of pyridine to **A** and **B** while perhaps the excess pyridine could also assist in a faster collapse of the two hydrides into the H_2 ligand (for instance through the effect of H-bonding).

Reversal of the relative rates of site exchange requires a new isomerisation pathway, resulting in selective migration of the axial H ligand in the square pyramidal geometry of **A** and **B** without moving the second H ligand in the equatorial plane. One attractive possibility for this transformation is a selective deprotonation of the axial site in **A** by excess pyridine, which is the strongest base present in solution, to yield a square planar monohydride intermediate $[RhH(\kappa^1\text{-P,S})(py)_2]$, followed by reprotonation at the opposite face of the square plane to afford **B**. This pathway is closely related to one of the proposed pathways for the H/D exchange between H_2 and solvent in pure CD_3OH (through intermediates **5** and **6** of Scheme 3). No calculations were carried out, however, to confirm the feasibility of this pathway. The fact that this strong effect is not observed during the transformation of the minor isomer into the major one (**8** → **9**) is consistent with the need to overcome the smaller $\mathbf{TS_{BD}}$ barrier in the first step to achieve the rapid site scrambling. Hence, if the transition state of the putative site-conserving concerted pathway is lower than $\mathbf{TS_{AC}}$ but higher than or comparable to $\mathbf{TS_{BD}}$, then the site exchange would remain operative even at low pyridine concentration. For the same reason, a very large concentration of pyridine does not afford a selective site inversion because collapse to the nonclassical intermediate promotes nonselective deprotonation.

Conclusions

The present contribution has explored the precatalyst activation phase for hydrogenation processes carried out in alcohol solvents with $[Rh(diene)(LL')]^+$ systems, using $[Rh(COD)(P,S^tBu)]^+$ as a model compound. The COD ligand is removed by hydrogenation to yield a putative $[Rh(P,S^tBu)(CH_3OH)_2]^+$ complex which promotes a very rapid H/D exchange between H_2 and the solvent, possibly *via* a dihydride species $[Rh(P,S^tBu)(H)_2(CH_3OH)_2]^+$ that is accessible according to the DFT calculations. Addition of L (pyridine or MeCN) slows down this exchange, allowing the observation of diastereomeric dihydride species at low temperature. Evidence has also been obtained for equilibrium deprotonation of these cationic dihydride complexes in the presence of strong bases (*e.g.* excess pyridine). This phenomenon is presumably linked to the need of a strong base promoter for the catalytic action of these compounds and of the iridium analogues in the ionic hydrogenation of polar unsaturated substrates.[14,22]

Acknowledgements

The York authors would like to thank the EPSRC (grant no. EP/G009546/1) for funding. The Toulouse and Moscow authors are grateful to the CNRS (Centre National de la Recherche Scientifique) and the RFBR (Russian Foundation for Basic Research) for support through the GDRI (Groupe de Recherche Internationale) "Homogeneous catalysis for Sustainable Development" and RFBR grants no. 12-03-93112, 12-03-31326, and 12-03-33018. We are also grateful to the IUF (Institut Universitaire de France) for additional funding and to the CINES (Centre Informatique National de l'Enseignement Supérieur) and the CICT (Centre Interuniversitaire de Calcul de Toulouse, project CALMIP) for granting free computational time. EMK thanks the Embassy of France in Moscow for a PhD grant.

Notes and references

1 J. A. Osborn, F. H. Jardine, J. F. Young and G. Wilkinson, *J. Chem. Soc. A*, 1966, 1711–1732.
2 R. H. Crabtree, H. Felkin and G. E. Morris, *J. Organomet. Chem.*, 1977, **141**, 205–215.
3 S.-M. Lu, X.-W. Han and Y.-G. Zhou, *Adv. Synth. Catal.*, 2004, **346**, 909–912.
4 S.-F. Zhu, J.-B. Xie, Y.-Z. Zhang, S. Li and Q.-L. Zhou, *J. Am. Chem. Soc.*, 2006, **128**, 12886–12891.
5 T. Imamoto, N. Iwadate and K. Yoshida, *Org. Lett.*, 2006, **8**, 2289–2292.
6 M. N. Cheemala and P. Knochel, *Org. Lett.*, 2007, **9**, 3089–3092.
7 G. Hou, F. Gosselin, W. Li, C. McWilliams, Y. Sun, M. Weisel, P. D. O'Shea, C.-Y. Chen, I. W. Davies and X. Zhang, *J. Am. Chem. Soc.*, 2009, **131**, 9882–9883.
8 W. J. Tang, J. Tan, L. J. Xu, K. H. Lam, Q. H. Fan and A. S. C. Chan, *Adv. Synth. Catal.*, 2010, **352**, 1055–1062.
9 W. Tang, Y. Sun, L. Xu, T. Wang, Q. Fan, K.-H. Lam and A. S. C. Chan, *Org. Biomol. Chem.*, 2010, **8**, 3464–3471.
10 D. Cartigny, T. Nagano, T. Ayad, J.-P. Genet, T. Ohshima, K. Mashima and V. Ratovelomanana-Vidal, *Adv. Synth. Catal.*, 2010, **352**, 1886–1891.
11 R. Dorta, D. Broggini, R. Stoop, H. Ruegger, F. Spindler and A. Togni, *Chem.–Eur. J.*, 2004, **10**, 267–278.
12 H.-U. Blaser, *Adv. Synth. Catal.*, 2002, **344**, 17–31.
13 L. Routaboul, S. Vincendeau, J.-C. Daran and E. Manoury, *Tetrahedron: Asymmetry*, 2005, **16**, 2685–2690.
14 E. Le Roux, R. Malacea, E. Manoury, R. Poli, L. Gonsalvi and M. Peruzzini, *Adv. Synth. Catal.*, 2007, **349**, 309–313.

15 R. Malacea, J.-C. Daran, S. B. Duckett, J. P. Dunne, C. Godard, E. Manoury, R. Poli and A. C. Whitwood, *Dalton Trans.*, 2006, 3350–3359.
16 R. Malacea, E. Manoury, L. Routaboul, J.-C. Daran, R. Poli, J. P. Dunne, A. C. Withwood, C. Godard and S. B. Duckett, *Eur. J. Inorg. Chem.*, 2006, 1803–1816.
17 A. Preetz, H. J. Drexler, C. Fischer, Z. Dai, A. Borner, W. Baumann, A. Spannenberg, R. Thede and D. Heller, *Chem.–Eur. J.*, 2008, **14**, 1445–1451.
18 A. Preetz, C. Fischer, C. Kohrt, H. J. Drexler, W. Baumann and D. Heller, *Organometallics*, 2011, **30**, 5155–5159.
19 E. Alberico, W. Baumann, J. G. de Vries, H. J. Drexler, S. Gladiali, D. Heller, H. J. W. Henderickx and L. Lefort, *Chem.–Eur. J.*, 2011, **17**, 12683–12695.
20 C. Fischer, S. Schulz, H. J. Drexler, C. Selle, M. Lotz, M. Sawall, K. Neymeyr and D. Heller, *ChemCatChem*, 2012, **4**, 81–88.
21 E. M. Kozinets, O. Koniev, O. A. Filippov, J.-C. Daran, R. Poli, E. S. Shubina, N. V. Belkova and E. Manoury, *Dalton Trans.*, 2012, **41**, 11849–11859.
22 E. M. Kozinets, N. V. Belkova, E. S. Shubina, R. Poli and E. Manoury, *Russ. Chem. Bull.*, 2013, 750–756.
23 S. B. Duckett and R. E. Mewis, *Acc. Chem. Res.*, 2012, **45**, 1247–1257.
24 R. A. Green, R. W. Adams, S. B. Duckett, R. E. Mewis, D. C. Williamson and G. G. R. Green, *Prog. Nucl. Magn. Reson. Spectrosc.*, 2012, **67**, 1–48.
25 C. R. Bowers and D. P. Weitekamp, *J. Am. Chem. Soc.*, 1987, **109**, 5541–5542.
26 T. C. Eisenschmid, R. U. Kirss, P. P. Deutsch, S. I. Hommeltoft, R. Eisenberg, J. Bargon, R. G. Lawler and A. L. Balch, *J. Am. Chem. Soc.*, 1987, **109**, 8089–8091.
27 K. Golman and J. S. Petersson, *Acad. Radiol.*, 2006, **13**, 932–942.
28 D. Blazina, S. B. Duckett, P. J. Dyson, B. F. G. Johnson, J. A. B. Lohman and C. J. Sleigh, *J. Am. Chem. Soc.*, 2001, **123**, 9760–9768.
29 D. Blazina, S. Duckett, P. Dyson and J. Lohmann, *Chem.–Eur. J.*, 2003, **9**, 1046–1061.
30 M. A. M. Al-Ibadi, S. B. Duckett and J. E. McGrady, *Dalton Trans.*, 2012, **41**, 4618–4625.
31 D. Schott, C. J. Sleigh, J. P. Lowe, S. B. Duckett, R. J. Mawby and M. G. Partridge, *Inorg. Chem.*, 2002, **41**, 2960–2970.
32 D. Schott, P. Callaghan, J. Dunne, S. B. Duckett, C. Godard, J. M. Goicoechea, J. N. Harvey, J. P. Lowe, R. J. Mawby, G. Müller, R. N. Perutz, R. Poli and M. K. Whittlesey, *Dalton Trans.*, 2004, 3218–3224.
33 J. Lopez-Serrano, S. B. Duckett, S. Aiken, K. Q. Almeida Lenero, E. Drent, J. P. Dunne, D. Konya and A. C. Whitwood, *J. Am. Chem. Soc.*, 2007, **129**, 6513–6527.
34 J. Lopez-Serrano, S. B. Duckett and A. Lledós, *J. Am. Chem. Soc.*, 2006, **128**, 9596–9597.
35 B. Eguillor, P. J. Caldwell, M. C. R. Cockett, S. B. Duckett, R. O. John, J. M. Lynam, C. J. Sleigh and I. Wilson, *J. Am. Chem. Soc.*, 2012, **134**, 18257–18265.
36 S. B. Duckett and C. J. Sleigh, *Prog. Nucl. Magn. Reson. Spectrosc.*, 1999, **34**, 71–92.
37 M. J. Frisch, G. W. Trucks, H. B. Schlegel, G. E. Scuseria, M. A. Robb, J. R. Cheeseman, G. Scalmani, V. Barone, B. Mennucci, G. A. Petersson, H. Nakatsuji, M. Caricato, X. Li, H. P. Hratchian, A. F. Izmaylov, J. Bloino, G. Zheng, J. L. Sonnenberg, M. Hada, M. Ehara, K. Toyota, R. Fukuda, J. Hasegawa, M. Ishida, T. Nakajima, Y. Honda, O. Kitao, H. Nakai, T. Vreven, J. A. Montgomery Jr., J. E. Peralta, F. Ogliaro, M. Bearpark, J. J. Heyd, E. Brothers, K. N. Kudin, V. N. Staroverov, R. Kobayashi, J. Normand, K. Raghavachari, A. Rendell, J. C. Burant, S. S. Iyengar, J. Tomasi, M. Cossi, N. Rega, N. J. Millam, M. Klene, J. E. Knox, J. B. Cross, V. Bakken, C. Adamo, J. Jaramillo, R. Gomperts, R. E. Stratmann, O. Yazyev, A. J. Austin, R. Cammi, C. Pomelli, J. W. Ochterski, R. L. Martin, K. Morokuma, V. G. Zakrzewski, G. A. Voth, P. Salvador, J. J. Dannenberg, S. Dapprich, A. D. Daniels, Ö. Farkas, J. B. Foresman, J. V. Ortiz, J. Cioslowski and D. J. Fox, *GAUSSIAN 09 (Revision A.01)*, Gaussian, Inc., Wallingford CT, 2009.
38 A. D. Becke, *J. Chem. Phys.*, 1993, **98**, 5648–5652.
39 C. T. Lee, W. T. Yang and R. G. Parr, *Phys. Rev. B: Condens. Matter*, 1988, **37**, 785–789.
40 Y. Zhao and D. G. Truhlar, *Theor. Chem. Acc.*, 2008, **120**, 215–241.
41 D. Andrae, U. Haussermann, M. Dolg, H. Stoll and H. Preuss, *Theor. Chim. Acta*, 1990, **77**, 123–141.
42 U. Haussermann, M. Dolg, H. Stoll, H. Preuss, P. Schwerdtfeger and R. M. Pitzer, *Mol. Phys.*, 1993, **78**, 1211–1224.
43 W. Kuchle, M. Dolg, H. Stoll and H. Preuss, *J. Chem. Phys.*, 1994, **100**, 7535–7542.
44 T. Leininger, A. Nicklass, H. Stoll, M. Dolg and P. Schwerdtfeger, *J. Chem. Phys.*, 1996, **105**, 1052–1059.
45 A. W. Ehlers, M. Boehme, S. Dapprich, A. Gobbi, A. Hoellwarth, V. Jonas, K. F. Koehler, R. Stegmann, A. Veldkamp and G. Frenking, *Chem. Phys. Lett.*, 1993, **208**, 111–114.
46 J. Fritsch and G. Zundel, *J. Phys. Chem.*, 1981, **85**, 556–561.
47 R. Kramer and G. Zundel, *J. Chem. Soc., Faraday Trans.*, 1990, **86**, 301–305.
48 M. Martin, E. Sola, O. Torres, P. Plou and L. A. Oro, *Organometallics*, 2003, **22**, 5406–5417.